Cunha, V.M.C.F.; Barros, J.A.O.; Sena Cruz, J.M. (2010) "Tensile behavior of steel fiber reinforced self-compacting concrete." SP-274-4 Fiber Reinforced Self-Consolidating Concrete: Research and Applications, ACI Committees 544 and 237, 51-68.

TENSILE BEHAVIOR OF STEEL FIBER REINFORCED SELF-COMPACTING CONCRETE

V. M. C. F. Cunha, J. A. O. Barros[1], J. M. Sena-Cruz

Synopsis: In the present work the tensile behavior of a self-compacting concrete reinforced with two hooked ends steel fiber contents was assessed performing stable displacement control tension tests. Based on the stress-displacement curves obtained, the stress-crack width relationships were derived, as well as the energy dissipated up to distinct crack width limits and residual strengths. The number of effective fibers bridging the fracture surface was determined and was compared with the theoretical number of fibers, as well as with the stress at crack initiation, residual stresses and energy dissipation parameters. In general, a linear trend between the number of effective fibers and both the stress and energy dissipation parameters was obtained. A numerical model supported on the finite element method was developed. In this model, the fiber reinforced concrete is assumed as a two phase material: plain concrete and fibers randomly distributed. The plain concrete phase was modeled with 3D solid finite elements, while the fiber phase was modeled with discrete embedded elements. The adopted interface behavior for the discrete elements was obtained from single fiber pullout tests. The numerical simulation of the uniaxial tension tests showed a good agreement with the experimental results. Thus, this approach is able of capturing the essential aspects of the fiber reinforced composite's complex behavior.

Keywords: FEM, Steel fiber reinforced self-compacting concrete; uniaxial tensile behavior.

[1] Author to whom the correspondence should be sent (barros@civil.uminho.pt).

Cunha, V.M.C.F.; Barros, J.A.O.; Sena Cruz, J.M. (2010) "Tensile behavior of steel fiber reinforced self-compacting concrete." SP-274-4 Fiber Reinforced Self-Consolidating Concrete: Research and Applications, ACI Committees 544 and 237, 51-68.

Vítor Cunha is a PhD Student in the Institute for Sustainability and Innovation in Structural Engineering (ISISE), Portugal. His main interests are the experimental characterization of steel fiber reinforced self-compacting concrete (SFRSCC), and FEM-based numerical modeling of SFRSCC structures.

Joaquim Barros is an ISISE member, Associate Professor of the Structural Division of the Dep. of Civil Engineering, University of Minho. He is a member of ACI Committees 440 and 544, a member of TG 8.3 and *fib* TG 9.3, and a Council member of the IIFC. His research interests include structural strengthening, composite materials, fiber reinforced concrete and the development of constitutive models for the FEM analysis.

José Sena Cruz is an ISISE member, Auxiliary Professor of the Structural Division of the Dep. of Civil Engineering, University of Minho. He is the secretary of the RILEM TC DUC. His main interests are the experimental and the numerical research of fiber reinforced concrete and composite materials for the structural strengthening.

Cunha, V.M.C.F.; Barros, J.A.O.; Sena Cruz, J.M. (2010) "Tensile behavior of steel fiber reinforced self-compacting concrete." SP-274-4 Fiber Reinforced Self-Consolidating Concrete: Research and Applications, ACI Committees 544 and 237, 51-68.

INTRODUCTION

Self-Compacting Concrete (SCC) can be defined as a concrete that is able to flow in the interior of the formwork, filling it in a natural manner and passing through the reinforcing bars and other obstacles, flowing and consolidating under the action of its own weight (Okamura 1997). Discrete steel fibers are added to cement based materials to increase their post-cracking residual strength, energy dissipation capacity and impact resistance (ACI 1996). The advantages associated to the addition of steel fibers to concrete mixes may be combined with the ones resulting from the self-compacting ability concept in concrete. The resulting material is designated by Steel Fiber Reinforced Self-Compacting Concrete (SFRSCC) and, when compared to conventional concretes, presents clear technical advantages in terms of costs/benefits ratio and an enhanced post-cracking behavior.

To explore the potentialities of SFRSCC for structural applications, mainly for the development of innovative systems in the precasting industry (Barros *et al.* 2007), a research project has being carried out evolving experimental, analytical and numerical research. With the purpose of getting, as much as possible, a consistent understanding of the behavior of this composite material, and to collect data for the calibration of the analytical formulations and FEM-based numerical models, the experimental research covers the micromechanics aspects of the fiber pullout (Cunha *et al.* 2006, 2008), the compressive (Cunha *et al.* 2008b) and flexural behavior (Pereira *et al.* 2008) and, more recently, the uniaxial tensile behavior.

The present work is dedicated to the characterization of the tensile behavior of two SFRSCC mixes, one reinforced with 30 kg/m^3 [1.873 lb/ft^3] and the other with 45 kg/m^3 [2.809 lb/ft^3] of hooked end steel fibers. From the stress-displacement curves, the stress-crack width relationships were derived and the values of parameters that characterize the residual strength and energy absorption for certain crack width limits were determined. The relevant aspect of the fiber distribution in SCC mixtures was also assessed comparing the values of these parameters determined in specimens extracted from top and bottom zones of SFRSCC elements. The influence of the number of effective fibers crossing the fracture surface in terms of the values of the parameters that characterize the post-cracking behavior of SFRSS was also assessed.

Finally, taking into account the force-slip relationships obtained in pullout tests with steel fibers of distinct inclination and embedded bond length, a numerical approach was developed assuming SFRSCC as a two phase material: SCC and fibers. SCC is simulated by a 3D multi-fixed smeared crack model developed by Ventura *et al.* (2008), while fibers are modeled as discrete embedded cables, whose internal forces are obtained from the force-slip relationships recorded in pullout tests, taking into account the inclination between fiber and the neighbor crack plane formed in the surrounding SCC, as well as an adopted average value for the fiber embedded length. In this approach it is assumed that the slip is equal to the crack width, which is determined multiplying the crack strain normal to the crack by the crack band width (Ventura *et al.* 2008). The present work describes the experimental work concerning to the characterization of the uniaxial tensile behavior of the developed SFRSCC. A brief description of the numerical model is done and its predictive performance is assessed.

RESEARCH SIGNIFICANCE

Structural applications of SFRC are yet to some extent limited, if having in mind that the appearance of SFRC dates back to the early sixties (ACI 1996). The high scatter of the SFRC material behavior, in part due to non-uniform fiber distribution, contributes to the mistrust in this material. In order to overcome these doubts it is of vital importance reducing the material behavior scatter, and consequently enabling the adoption of lower material safety factors (Shah and Ferrara 2008). Self-compacting concrete is effective in guaranteeing a more uniform distribution of fibers within the specimen, as well in effectively orienting them along the casting direction. Nowadays, it is acknowledge that SFRSCC exhibits better post-cracking behavior with a lower scatter than conventional SFRC.

In this paper, the post-cracking behavior of SFRSCC obtained from uniaxial tensile tests is presented. The results are discussed based upon the micro-mechanical behavior of the steel fibers used in the composition. The fibers micro-mechanical behavior was previously assessed by means of single fiber pullout tests (Cunha *et al.* 2008b). The knowledge of the micro-mechanical behavior enables a deeper understanding of the composite behavior, which often lacks in the discussion of the experimental results presented in the available literature.

The numerical model developed and employed to simulate the SFRSCC's uniaxial tensile behavior assumes the composite as a two phase material: SCC (paste and aggregates) and fibers. The random fiber distribution into the matrix is simulated with an algorithm supported on the Monte Carlo method, providing a realistic distribution of the fibers in a certain specimen. The numerical fiber distribution generated takes into account mould and fiber dimensions. This enables to consider the so-called wall effect in distinct ways depending on the mould shape and geometry. With a realistic approximation of the actual fiber distribution and with the knowledge of the micro-mechanical behavior of the fibers, it was possible to predict the macro-mechanical behavior of laboratory's specimens. The presented numerical approach is not yet fully validated, however the results are promising and its application to other structural elements of fiber reinforced concrete with complex geometry may be, in the future, easily achieved with good results.

MATERIALS AND SPECIMENS

The materials and mixture procedures used for the SFRSCC are described elsewhere (Pereira *et al.* 2008). Two batches with distinct contents of fibers (Cf), 30 and 45 kg/m^3 [1.873 and 2.809 lb/ft^3] were used to study the SFRSCC tensile post-cracking behavior. Table 1 includes the composition that has best fitted self-compacting requirements for the adopted two fiber contents. Remark that, in Table 1, WS is the water necessary to saturate the aggregates, and W/C is the water/cement ratio. The WS portion was not used to compute the W/C ratio. Hooked-ends steel fibers (length, l_f = 60 mm [1.181 in], diameter, d_f = 0.75 mm [0.0216 in], with an aspect ratio, l_f / d_f = 80, and yield stress of 1100 MPa [159542 psi]) were used for the study.

For each batch, eight cylinders with a diameter of 150 mm [5.905 in] and 300 mm [11.810 in] height were cast. Three of them were used to assess the compressive strength of each SFRSCC batch. At the date when the tests were performed, the series with 30 kg/m^3 [1.873 lb/ft^3] of fibers had an average compressive strength of 71.1 MPa [10312 psi] with a coefficient of variation, CoV, of 1.9 %, while in the series with 45 kg/m^3 [2.809 lb/ft^3] of fibers the SFRSCC had an average compressive strength of 67.2 MPa [9747 psi] with a CoV of 1.4 %.

TEST SETUP

The RILEM TC 162-TDF (2001) recommendations for the uniaxial tension test of steel fiber reinforced concrete were adopted in this work. According to this document, a notched cylinder of both 150 mm [5.905 in] diameter and height should be used. The specimens were swan out from standard cylinders having a height of 300 mm [11.810 in]. Afterwards, a notch along the perimeter with a 15 mm [0.591 in] depth and 5 mm [0.197 in] thick was swan at mid height of the final test specimen. When the sawn operations were executed, the specimens were in its hardened-mature phase. These operations were conducted with care in order to ensure that the notch become perpendicular to the specimen's axis.

Afterwards, each specimen was ground and carefully cleaned with both compressed air and solvent. The specimen was then directly glued, "in situ", to the loading platens of the testing rig. The selected glue is a high strength epoxy resin, which achieves a tensile strength of about 30 MPa [4351 psi] and a bound strength between 4 to 8 MPa [580 to 1160 psi] (depending on the surface material and treatment characteristics).

A servo-hydraulic system with a 2000 kN [449618 lb] static load carrying capacity with a very stiff frame was used to perform the tensile tests, Figure 1a. A test was performed in closed-loop displacement control using the average signal of three displacement transducers mounted on two steel rings disposed at equal distances along the perimeter of the specimen, Figure 1b. The gauge length adopted was 35 mm [1.378 in], smaller than the upper limit length of 40 mm [1.575 in] suggested by RILEM TC 162-TDF (2001). The following displacement rates were used: 5 μm/min [0.000196 in/min] up to a displacement of 0.1 mm [0.00394 in]; 100 μm/min [0.00394 in/min] until the completion of the test, i.e. a 2 mm [0.0787 in] displacement.

RESULTS

Stress-displacement curves

In all the uniaxial tension tests performed, cracking occurred along the notched plane, hence the desired crack localization was assured. The average curve and the envelope of the experimental uniaxial tension stress - average displacement relationships, σ - δ_{avg}, for a fiber content of 30 and 45 kg/m^3 [1.873 and 2.809 lb/ft^3] are presented in Figures 2 and 3, respectively. Hereinafter, these series will be designated by Cf30 and Cf45, respectively. A detailed view of the initial part of the experimental response is depicted on the right side of these figures. For both tested series the σ - δ_{avg} response is linear almost up to peak. Only just before the peak load some non-linearity is observed. Once the peak load is attained, the load had a relatively accentuated decrease up to a displacement of about 0.10 mm [0.00394 in] (see right side of both Figures 2 and 3). Beyond this displacement value, a plateau or a hardening-plastic response has occurred. In general, the post-peak hardening is observed in the Cf45 series, but this response was also occurred in some specimens of the Cf30 series (Cunha 2009). On the other hand, after the plateau on the Cf30 series, i.e. beyond a displacement of nearby 0.8 mm [0.0315 in], the residual stress starts to decrease with sudden strength losses corresponding to the fiber fracture. In fact, during the execution of the tension tests, this was audible by the peculiar sound of fiber fracturing.

According to Stroeven and Hu (2006), the average orientation angle of the active fibers crossing a leading crack is 35^o (this value was analytically derived), and a similar value (34^o) was experimentally observed by Soroushian and Lee (1990). Recent fiber pullout tests with fibers at an inclination angle of 30^o with the load direction have conducted to fiber rupture; the predominant failure mode occurred when the slip was in the range [0.6-1.0] mm [Cunha et al 2006]. These reasons can justify the occurrence of the significant residual stress decay after the displacement of 0.8 mm [0.0315 in], in Cf30 series, where the number of active fibers is relatively reduced for the strength of the matrix.

Concerning the Cf45 series (Figure 5), the post-peak hardening observed can be ascribed to two reasons: a higher number of active fibers crossing the crack; notice that both the compressive strength and stiffness of the Cf45 series matrix are lower than the Cf30, thus the fiber-matrix bond properties are not so favorable to proportionate fiber rupture. After the peak load, the stress starts to decrease until a minimum stress is attained, roughly about 0.1 mm [0.00394 in]. As micromechanics of hooked-ends fiber pullout demonstrate (Cunha 2009), above this displacement, the strengthening provided by fiber hooked-ends starts to be the predominant fiber reinforcement mechanism. Since there are more fibers intersecting the crack, and due to the lower tensile strength of the concrete, the energy released during cracking is smaller when compared to the Cf30 series. Moreover, due to the lower tensile strength and matrix stiffness, fibers did not fracture so often as in the Cf30 series. Consequently, beyond a displacement around 0.1 mm [0.00394 in] a hardening phase occurred up to a displacement value of about 1.0 mm [0.0394 in].

In general, the responses exhibit very low scatter in the pre-peak phase. On the other hand, in the post-peak branch the scatter was considerably higher, particularly in Cf30 series and for a displacement higher than 0.1 mm [0.00394 in]. Up to 0.1 mm [0.00394 in] the commanding pullout reinforcement mechanism is the chemical bond (Cunha 2009), hence the influence of the fiber dispersion (implicitly orientation) is not so important. As the crack width increases, the fiber's hooked-ends start to be mobilized. Hence, the scatter of the post-peak behavior increases due to the variation of the fiber dispersion between different specimens, namely, the fiber orientation. Moreover, for the Cf30 series, fiber rupture was the predominant fiber failure mode, as it was expected taking into account the results obtained in fiber pullout tests presented elsewhere (Cunha *et al.* 2006).

Stress-crack opening curves

Figures 4 and 5 present the envelope of the stress-crack width curves obtained in the tests for the Cf30 and Cf45 series, respectively. A stress crack width curve (σ - w) was derived from a stress displacement curve (σ - δ) according to the recommendations of RILEM TC 162- TDF (2001). The average and the characteristic σ - w curves are also included in these figures. The characteristic σ - w curve for the lower bound (L.B.) and upper bound (U.B.) with a confidence level of k = 95% was obtained from the average curve computed from all tests, $\bar{\sigma}_w(w)$, according to RILEM TC 162-TDF (2001):

$$\sigma_{w,k}(w) = \bar{\sigma}_w(w)\frac{G_{F2mm,k}}{\bar{G}_{F2mm}} \qquad (1)$$

where $\bar{G}_{F2mm}$ is the average energy dissipated up to a crack width of 2 mm [0.0787 in] and $G_{F2mm,k}$ is the characteristic energy dissipated for the same crack width. To compute $G_{F2mm,k}$ a t-Student distribution was assumed.

Stress and toughness parameters

The average and characteristic values of the stresses and toughness parameters, as well as the respective coefficients of variation obtained from the performed uniaxial tests, are included in Table 2. In this Table σ_{peak} is the maximum stress, while $\sigma_{0.3mm}$, σ_{1mm} and σ_{2mm} are the stress at a crack width values of 0.3, 1 and 2 mm, respectively [0.0118, 0.0394 and 0.0787 in]. On the other hand, G_{F1mm} and G_{F2mm} represent the dissipated energy up to a crack width of 1 and 2 mm, respectively [0.0394 and 0.0787 in]. The characteristic values were obtained for a k=95% confidence level assuming a t-Student distribution. The normality of the sample was ascertained by the Shapiro-Wilk test (Montgomery and Runger 1994). The number of total fibers, N_f, and effective fibers, N_f^{eff}, counted at the fracture surface are also included in Table 2. Effective fibers were considered all the fibers that had the end hook deformed, as well as the fibers that have ruptured. In spite of some researchers do not consider the ruptured fibers as "effective", in the authors' opinion they should be considered, since they are able to transfer forces between the crack surfaces up to reasonable crack width. The "fully effectiveness" of this type of fibers can be questionable, but it is feasible to admit that they are "partially effective". For the simplicity sake, let's assume that the fiber slip when it is being pulled out is approximately equal to the crack width. Then, as it can be observed in Cunha *et al*. (2006) work, in the pullout behavior of inclined fibers, depending on the inclination angle and embedded length, a fiber that fails by rupture can sustain forces up to a slip, i.e. crack width that varies approximately from 0.7 mm [0.0276 in] to 4 mm [0.157 in].

From the analysis of Table 2 it is verified that, in general, the stresses and toughness parameters increased with the fiber content, as it would be expected. The only exception was the peak stress which was nearby 10 % lower for the series with a content of fibers of 45 kg/m^3. Remark that this decrease is not due to the content of fiber, even though it could be indirectly appointed to it, since the aggregates, cement and additions contents for each series are distinct in order to attain self-compactability requirements. Moreover, the peak stress cannot be regarded as the actual tensile strength, but as estimation. In fact the notched forced a stress concentration at the notch tip, forcing the crack to be localized in the notched plan, which could not be the weakest section of an unnotched specimen (Van Mier and Van Vliet, 2002).

A significant increase of the post-cracking stresses was observed with the higher fiber content. An increase of the fiber content of 15 kg/m^3 [0.936 lb/ft^3] increased the residual strengths from 2 to 7 times, depending on the crack width value. Such increase is not simply justified by the higher number of fibers crossing the crack surface for the Cf45 series, since there are other factors that contributed to this fiber reinforcement effectiveness. One of these factors is the predominant fiber failure mode that, as already mentioned, was fiber rupture in the Cf30 series and fiber pullout in Cf45 series.
As far as the dissipated energy (G_F) is concerned, in the Cf45 series a significant increase (2 to 2.6 times) up to both deflections of 1 and 2 mm [0.0394 and 0.0787 in] was observed. In general, the CoV values obtained for the G_F parameters were considerably smaller for the Cf45 series. At a first glance, these values may seem relatively high; the magnitude of such values is, however, within the expected values for this type of material. In fact, in general, the obtained CoV values were smaller than the ones reported by other authors with the same test procedure and specimen's dimensions for conventional fiber reinforced concrete (Barragan 2002, Läofgren *et al*. 2008).

In Figure 6 is depicted the relationship between the total number of fibers, N_f (Cunha 2009), and the number of effective fibers, N_f^{eff}, at the fracture surface obtained for all the tested specimens of both Cf30 and Cf45 series. Since the uniaxial tension test specimens (with 150 mm [5.905 in] height) were obtained from distinct parts of a standard cylinder with 300 mm [11.810 in] height, additionally, the specimens obtained from the bottom and upper part of the standard cylinder are distinguished in Figure 6. This process enables an indirect assessment of an eventual influence of the material specific weight (gravity) on the fiber distribution. Figure 6 shows a linear relationship between the N_f and N_f^{eff}. Moreover, a tendency for an eventual higher concentration of fibers in the bottom part of the specimen was not found. Dupont (2003) has also found a linear relationship between the total

number of fibers and the number of effective fibers for small fiber contents. However, for higher fiber contents this relationship becomes nonlinear, with an increase of N_f^{eff} as smaller as higher is N_f. In fact, due to the group effect, N_f^{eff} may decrease as the fiber spacing decreases due to the higher probability of mutual influence of adjacent fibers (Naaman and Shah 1976).

Influence of the number of effective fibers on the post-cracking parameters

Throughout Figures 7a to 7f are depicted the relationships between N_f^{eff} and the aforementioned post-cracking parameters obtained from the uniaxial tension test. Regarding the peak stress, σ_{peak}, no significant relation was observed with the N_f^{eff} increase (Figure 7a). In spite of σ_{peak} for the Cf45 series has been, in general, smaller than for Cf30 series, due to the reasons already pointed out, there was no significant relation between σ_{peak} and the origin of specimen, i.e. from lower or upper part of a standard cylinder. This suggests that there was no significant segregation of the matrix skeleton and paste in the casted cylinders. On the other hand, for the residual stresses at a crack width of 0.3 mm [0.0118 in], $\sigma_{0.3mm}$, and 1 mm [0.0394 in], σ_{1mm}, a linear relationship between these residual stresses and the N_f^{eff} is quite evident (Figures 7b and 7c). This was expected, since the residual stress sustained by the crack is intimately related to number of mobilized fibers. Concerning the Cf45 series, the residual stresses for the "top specimens" exhibited a lower scatter when compared to the values from the "bottom specimens". Due to technical problems occurred during the test program, the number of specimens from the bottom part (5) was different of the specimens obtained from the top part of the standard cylinder (3); therefore, no conclusive elations could be withdrawn in this subject.

The relation between the residual stress at a crack opening of 2 mm [0.0787 in], σ_{2mm}, and the N_f^{eff} is represented in Figure 7d. When compared to the $\sigma_{0.3mm}$ - N_f^{eff} and σ_{1mm} - N_f^{eff} relationships, the overall trend differed. First of all, there are two clear distinct trends for the σ_{2mm} - N_f^{eff} relationship. For the Cf30 series, the increase of σ_{2mm} with N_f^{eff} is marginal and can be assumed null. On the other hand, for the Cf45 series a linear increase of σ_{2mm} with N_f^{eff} is quite visible, in spite of a higher scatter than those register for the $\sigma_{0.3mm}$ - N_f^{eff} and σ_{1mm} - N_f^{eff} relationships. Moreover, a clear jump on the σ_{2mm} value from the series Cf30 to Cf45 is visible, even though there is a small difference of N_f^{eff} between the Cf30 series' specimen with the highest N_f^{eff} and the Cf45 series with the lowest N_f^{eff}. This considerable jump on σ_{2mm} value from the Cf30 to Cf45 specimens is not ascribed to the increase of effective fibers, hence this jump comprises differences on the fiber micro-mechanical behavior between the two series with distinct fiber content, as previously stated. In fact, for the series Cf30, in general, the fibers ruptured before a 2 mm [0.0787 in] crack width, while in case of Cf45 series, in general, the fibers were fully pulled-out enabling a higher crack bridging stress transfer effectiveness.
Finally, in both series and regardless the extracting location of the specimen, the dissipated energy has shown a linear increase with N_f^{eff}, for both considered crack width limits. Nevertheless, there are two aspects that should be emphasized. For the energy dissipated up to a 2 mm [0.0787 in] crack width, G_{F2mm}, there is also a jump on the G_{F2mm} value from the Cf30 to Cf45 series for the same reasons pointed for the σ_{2mm} - N_f^{eff} relationship. The other aspect is that the increment rate of both G_{F1mm} and G_{F2mm} with N_f^{eff}, for the Cf45 series, was slightly smaller than for Cf30 series.

NUMERICAL SIMULATION

Numerical model

In steel fiber reinforced cementitious composites (SFRC), steel fibers and matrix are bonded together through a weak interface, which behavior is important to understand the mechanical behavior of SFRC, since properties of the composite are greatly influenced by this interface zone (Pereira 2006). Taking this into account and that the fiber contribution for the post-cracking behavior of a composite is significantly higher than the unreinforced matrix

contribution, it was settled to model the SFRC as a two phase material. In the developed model, SFRC is treated as a heterogeneous medium comprised by one homogeneous phase (aggregates and paste), and another one composed by the steel fibers. The fracture process of the cementitious matrix (unreinforced) is modeled with a 3D multi-fixed smeared crack model. The formulation of this crack model can be found elsewhere (Ventura *et al*. 2008). On the other hand, the stress transfer between crack planes due to the fibers bridging an active crack is modeled with discrete embedded elements. A nonlinear behavior law is assigned to these elements in order to account the fiber-matrix interface properties.

The random fiber distribution into the matrix is simulated with an algorithm supported on the Monte Carlo method, providing a realistic distribution of the fibers in a certain specimen. The geometry, location and orientation of the fibers are subsequently inserted in a three dimensional finite element mesh. This approach was adopted, mainly, due to the following reasons: 1) a homogenization of the reinforcements (fibers) crossing a certain solid element is difficult due to the random nature of the fiber distribution; 2) the discrete modeling of the reinforcements as bar elements located along the solid element nodes leads to a higher computational cost due to an unnecessary concrete mesh refinement. Moreover, this mesh refinement could lead to numerical errors caused by distorted elements for comprising the fiber distribution.

The contribution of the steel fibers crossing a solid volume is given by:

$$K^{rc} = K^{c} + \sum_{i=1}^{nf} K_i^{f} \qquad (2)$$

where K^{rc}, K^{c} and K_i^{f} are, respectively, the stiffness matrix of the reinforced solid element (plain concrete + fiber reinforcement contribution), the stiffness matrix of plain concrete and the stiffness matrix of the i^{th} embedded fiber; n_f is the total number of fibers crossing the "mother" element.

A tri-linear stress-strain (σ-ε_{cable}) diagram was used for modeling the fibers' bond-slip behavior. This relationship was obtained from fiber pullout tests carried out for three distinct inclinations angles, α, (0º, 30º and 60º). In Figure 8 is depicted the procedure adopted to obtain the σ-ε_{cable}, where ε_{cable}, s and l_b are, respectively, the embedded cable strain, the crack band-width and the steel fiber's slip; σ is stress computed from the pullout force, P, divided by the fibre's cross sectional area, A_f. The tension-strain law assigned to each embedded cable depends on the inclination angle, θ, between the cable and the normal vector of the active crack surface, $\hat{n}$ (see Figure 9).

Simulations

The model performance is appraised by simulating the uniaxial tension tests already presented in this work. In Figures 10a and 10b are depicted, respectively, the mesh used exclusively for the concrete matrix phase and the three-dimensional mesh used for modeling the self-compacting concrete with the steel fiber contribution (Cf30 series).

In the present mesh, Lagrangian 8-noded solid elements are used for modeling the plain concrete contribution. Since the specimen had a notch at its mid-height, all the non-linear behavior was localized at the notch region, thus a 2×2×1 Gauss-Legendre integration scheme is used (1 integration point in the loading direction). The remaining solid elements are modeled with linear elastic behavior, and a 2×2×2 Gauss-Legendre integration scheme is adopted. The Cornelissen *et al.* (1986) softening law was used for modeling the nonlinear behavior of SCC. The material properties of the plain concrete matrix used in the simulations are included in Table 3. These values were obtained taking into account the strength class registered for the Cf30 and Cf45 series.

On the other hand, the steel fibers are modeled with 3D embedded elements with two integration points (Gauss-Legendre). A nonlinear behavior is assumed for all the embedded elements. From the fiber pullout tests were ascertained three distinct σ-ε_{cable} laws corresponding, respectively, to the studied fiber pullout inclination angles, α, (0º, 30º and 60º). Due to the impossibility of having a σ-ε_{cable} law for every possible inclination angle, the σ-ε_{cable} laws obtained from the pullout tests with an angle α of 0º, 30º and 60º was assigned, respectively, to the embedded cables with an orientation towards the active crack surface (θ) ranging from [0º, 15º[, [15º, 45º[and [45º, 75º].

Figures 11 and 12 present the numerical simulation of the uniaxial tension tests of the Cf30 and Cf45 series, respectively. For the Cf30 series the results of the numerical simulations were in agreement with the experimental results. The predicted numerical tensile strength is nearby the upper bound limit of the experimental envelope. This is feasible since, during testing, is almost impossible to completely exclude eccentricities, thus the experimental post-cracking average strength is smaller than the correspondent numerical one. For the Cf45 series, two numerical simulations were carried out. The first one adopting the σ-ε_{cable} laws obtained from the fiber pullout tests (in which fiber rupture was observed for a α=30º and 60º). Up to a crack width of approximately 1.0 mm [0.0394 in], a fairly good agreement with the experimental response is observed. Significant stress decay is, however, observed after this crack width limit due, mainly, to the rupture of the embedded cables with an inclination θ between 15º and 45º. It should be noticed that, the embedded cables with an inclination θ between 45º and 75º have also rupture, but only for crack widths higher than 2 mm. Since for the uniaxial tension tests of Cf45 series, fiber rupture did not occur so often, due to lower matrix strength and a higher number of fibers crossing the crack's fracture surface, another simulation was carried out assuming that the embedded cables with an inclination θ between 15º and 45º did not rupture. Assuming that fibers did not rupture, for Cf45 series; the quality of the simulation was improved. (Figure 12).

Cunha, V.M.C.F.; Barros, J.A.O.; Sena Cruz, J.M. (2010) "Tensile behavior of steel fiber reinforced self-compacting concrete." SP-274-4 Fiber Reinforced Self-Consolidating Concrete: Research and Applications, ACI Committees 544 and 237, 51-68.

CONCLUSIONS

In the present work the tensile behavior of self-compacting concrete (SCC) reinforced with two distinct hooked ends steel fiber contents (30 and 45 kg/m^3 [1.873 and 2.809 lb/ft^3]) was characterized by performing displacement controlled tensile tests.

The stress-crack opening relationships were derived from the stress-displacement curves. Additionally, the residual stress and energy dissipation parameters able of indicating the effectiveness of fiber reinforcement mechanisms in these two composite materials were determined. The relatively high compactness of the matrix system of these SFRSCC, the number of effective fibers bridging the fracture surface and the results obtained in a previous research program dealing with fiber pullout behavior of this type of steel fibers were all taken into account to interpret the post-cracking tensile behavior of the tested composites. In general, a linear relationship between the post-cracking parameters and the number of effective fibers was observed. A strong dependency on the type of fiber failure mode and the stiffness of the matrix and number of effective fibers was detected, which justified the occurrence of a pseudo-hardening branch in the softening phase of the SFRSCC with the highest fiber content (Cf45 series), as well as the significant residual strength decay occurred in the SFRSCC with the lowest fiber content (Cf30). In fact, in Cf45 series the predominant failure mode was fiber pullout, while in Cf30 series fiber rupture was the main failure mode.

The SFRSCC tensile behavior was numerically modeled as a two phase material. The matrix was simulated with a 3D multi-fixed smeared-crack model, while fibers were modeled as discrete embedded short cables distributed into the concrete matrix FE-mesh according to a Monte Carlo method. A good agreement between the numerical and experimental results was obtained.

ACKNOWLEDGEMENTS

The first author acknowledges the support provided by the grant SFRH/BD/18002/2004. The study reported in this paper forms a part of the research program "PONTALUMIS - Development of a prototype of a pedestrian bridge in GFRP-ECC concept", Project nº 3456, QREN. The Authors also acknowledge the support of Civitest Company on the production of the SFRSCC specimens.

Cunha, V.M.C.F.; Barros, J.A.O.; Sena Cruz, J.M. (2010) "Tensile behavior of steel fiber reinforced self-compacting concrete." SP-274-4 Fiber Reinforced Self-Consolidating Concrete: Research and Applications, ACI Committees 544 and 237, 51-68.

REFERENCES

ACI Committee 544, 1996, "State-of-the-art report on fiber reinforced concrete (ACI 544.1R)," American Concrete Institute.

Barragan, B. E., 2002, "Failure and Toughness of Steel Fiber Reinforced Concrete under Tension and Shear," Ph.D. thesis, Universitat Politecnica de Catalunya, Barcelona, Spain, 272 pp.

Barros, J.A.O.; Pereira, E.B.; Santos, S.P.F., 2007, "Lightweight panels of steel fiber reinforced self-compacting concrete," *Journal of Materials in Civil Engineering*, V. 19, No. 4, pp. 295-304.

Cornelissen, H.A.W.; Hordijk, D.A.; Reinhardt, H.W., 1986, "Experimental determination of crack softening characteristics of normalweigth and lightweight concrete," *Heron*, Fracture Mechanics and Structural Aspects of Concrete, Vol. 31, No. 2, pp. 45-56.

Cunha, V.M.C.F., "Steel Fibre Reinforced Self-Compacting Concrete – from Micromechanics to Composite behavior," Ph.D thesis, University of Minho (submitted).

Cunha, V.M.C.F.; Barros, J.A.O.; Sena-Cruz, J.M., 2008b, "Modelling the influence of age of steel fibre reinforced self – compacting concrete on its compressive behavior," *Materials and Structures Journal*, V. 41, No. 3, pp. 465-478.

Cunha, V.M.C.F.; Barros, J.A.O.; Sena-Cruz, J.M., 2008a, "Analytical model for bond-slip of hooked-end steel fibres," *Proceedings of the Conference Challenges for Civil Construction International Conference - CCC2008*, Porto, Portugal, 12 pp.

Cunha, V.M.C.F.; Barros, J.A.O.; Sena-Cruz, J.M., 2006, "Pullout behaviour of hooked-end steel fibers in self-compacting concrete," *Technical report 07-DEC/E-06*, Department of Civil Engineering, University of Minho, 88 pp.

Dupont, D., 2003, "Modeling and experimental validation of the constitutive law (σ-$\in$) and cracking behaviour of steel fibre reinforced concrete," PhD thesis, Department of Civil Engineering, Catholic University of Leuven, Belgium.

Läofgren, I.; Stang, H.; Olesen, J. F., 2008, "The WST method, a fracture mechanics test method for FRC," *Materials and Structures*, V. 41, pp. 197-211.

Montgomery, D. C.; Runger, G. C., 1994, *Applied statistics and probability for engineers*, John Wiley & Sons, Inc., Ney York, USA, 1024 pp.

Naaman, A.; Shah, S., 1976, "Pullout mechanism in steel fibre reinforced concrete," *Journal of the Structural Division*, V. 102, pp. 1537-1548.

Okamura, H., 1997, "Ferguson Lecture for 1996: Self-compacting high-performance concrete," *Concrete International*, V. 19, No. 7, pp. 50-4.

Pereira, E.B.; Barros, J.A.O., Camões, A.F.F.L., 2008, "Steel fiber reinforced self-compacting concrete – experimental research and numerical simulation," *Journal of Structural Engineering*, V. 134, No. 8, pp. 1310-1321.

Pereira, E.N.B., 2006, "Steel Fibre Reinforced Self-compacting Concrete: from material to mechanical behavior," dissertation for Pedagogical and Scientific Aptitude Proofs, Department Civil Engineering, University of Minho, 188 pp.

RILEM TC 162-TDF, 2001, "Test and design methods for steel fibre reinforced concretes: Uni-axial tension test for steel fibre reinforced concrete," *Journal of Materials and Structures*, V. 34, pp. 3-6.

Shah, S. P.; Ferrara, L., 2008, "Self consolidating fiber reinforced concrete," *Sevnth. Intnl. RILEM Symposium on Fibre Reinforced Concrete: Design and Applications*, 641-659. Chennai, India.

Soroushian, P.; Lee, C. D., 1990, "Distribution and orientation of fibers in steel fiber reinforced concrete," *ACI Materials Journal*, V. 87, No. 5, pp. 433-439.

Stroeven, P.; Hu, J., 2006, "Effectivness near boundaries of fibre reinforcement in concrete," *Materials and Structures*, V. 39, pp. 1001-1013.

Van Mier, J. G. M.; Van Vliet, M. R. A., 2002, "Uniaxial tension test for the determination of fracture parameters: state of the art," *Journal of Engineering Fracture Mechanics*, V. 69, pp. 235-247.

Ventura-Gouveia, A.; Barros, J.A.O.; Azevedo, A.F.M; Sena-Cruz, J.M., 2008, "Multi-fixed smeared 3D crack model to simulate the behaviour of fibre reinforced concrete structures," *Proceedings of the Conference Challenges for Civil Construction International Conference - CCC2008*, Porto, Portugal, 11 pp.

Cunha, V.M.C.F.; Barros, J.A.O.; Sena Cruz, J.M. (2010) "Tensile behavior of steel fiber reinforced self-compacting concrete." SP-274-4 Fiber Reinforced Self-Consolidating Concrete: Research and Applications, ACI Committees 544 and 237, 51-68.

TABLES AND FIGURES

List of Tables:

Cunha, V.M.C.F.; Barros, J.A.O.; Sena Cruz, J.M. (2010) "Tensile behavior of steel fiber reinforced self-compacting concrete." SP-274-4 Fiber Reinforced Self-Consolidating Concrete: Research and Applications, ACI Committees 544 and 237, 51-68.

Table 1 — Composition for 1 m^3 of SFRSCC

Cement Type I 42.5R (C) [kg]	Limestone Filler (LF) [kg]	Water (W) [dm^3]	Water to saturate aggregates (WS) [dm^3]	Super plasticizer ($SP^{(1)}$) [dm^3]	Fine Sand (FS) [kg]	Coarse Sand (CS) [kg]	Crushed Calcareous (CA) [kg]	Steel Fibers (Cf) [kg]
359.4	312.2	96.9	64.7	6.9	108.2	709.4	665.2	30
401.7	344.2	117.3	65.4	7.6	178.3	668.1	668.1	45

(1) SP- Sika HE200P; 1 kg = 2.2 lbs; 1 dm^3 = 0.03531 ft^3; 1 mm = 0.0394 in.; 1m^3 = 6.1023×10^4 $in.^3$

Table 2 — Stress and toughness parameters obtained from the uniaxial tension tests [1 MPa = 146 psi; 1 N = 0.2248 lb; 1 mm = 0.0394 in]

Cf [kg/m^3]		N_f [-]	N_f^{eff} [-]	σ_{peak} [MPa]	$\sigma_{0.3mm}$ [MPa]	σ_{1mm} [MPa]	σ_{2mm} [MPa]	G_{F1mm} [N/mm]	G_{F2mm} [N/mm]
30	Avg.	27	19	3.392	0.649	0.520	0.186	0.685	1.007
	CoV	30.8%	28.8%	13.0%	36.6%	45.1%	22.8%	32.3%	33.7%
	$k_{95\%}$	20	14	3.024	0.450	0.324	0.250	0.500	0.724
45	Avg.	67	39	3.019	1.219	1.466	1.342	1.342	2.645
	CoV	16.1%	16.5%	9.9%	18.0%	12.7%	18.0%	13.6%	13.1%
	$k_{95\%}$	58	34	2.768	1.036	1.310	0.972	1.189	2.356

Cunha, V.M.C.F.; Barros, J.A.O.; Sena Cruz, J.M. (2010) "Tensile behavior of steel fiber reinforced self-compacting concrete." SP-274-4 Fiber Reinforced Self-Consolidating Concrete: Research and Applications, ACI Committees 544 and 237, 51-68.

Table 3 — Plain concrete properties used in the simulations [1 MPa = 146 psi; 1 N = 0.2248 lb; 1 mm = 0.0394 in]

Property	Series	
	Cf30	Cf45
Density	$\rho = 2.4\times10^{6}$ N/mm^3	
Poisson ratio	$\nu = 0.2$	
Initial Young modulus	41.3×10^{3} N/mm^2	40.6×10^{3} N/mm^2
Compressive strength	71.1 N/mm^2	67.2 N/mm^2
Tensile strength	4.6 N/mm^2	4.5 N/mm^2
Fracture energy	0.117 N/mm	0.114 N/mm
Crack band-width	l_b = 5 mm (equal to the element height at the notch)	
Threshold angle	30º	

Cunha, V.M.C.F.; Barros, J.A.O.; Sena Cruz, J.M. (2010) "Tensile behavior of steel fiber reinforced self-compacting concrete." SP-274-4 Fiber Reinforced Self-Consolidating Concrete: Research and Applications, ACI Committees 544 and 237, 51-68.

List of Figures:

Cunha, V.M.C.F.; Barros, J.A.O.; Sena Cruz, J.M. (2010) “Tensile behavior of steel fiber reinforced self-compacting concrete.” SP-274-4 Fiber Reinforced Self-Consolidating Concrete: Research and Applications, ACI Committees 544 and 237, 51-68.

(a)

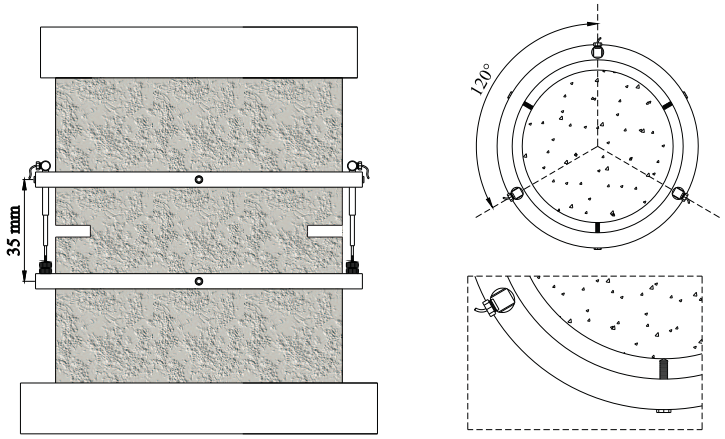

(b)

Figure 1 — Uniaxial tensile test setup: (a) general view and (b) location of displacement transducers (not scaled)

Cunha, V.M.C.F.; Barros, J.A.O.; Sena Cruz, J.M. (2010) "Tensile behavior of steel fiber reinforced self-compacting concrete." SP-274-4 Fiber Reinforced Self-Consolidating Concrete: Research and Applications, ACI Committees 544 and 237, 51-68.

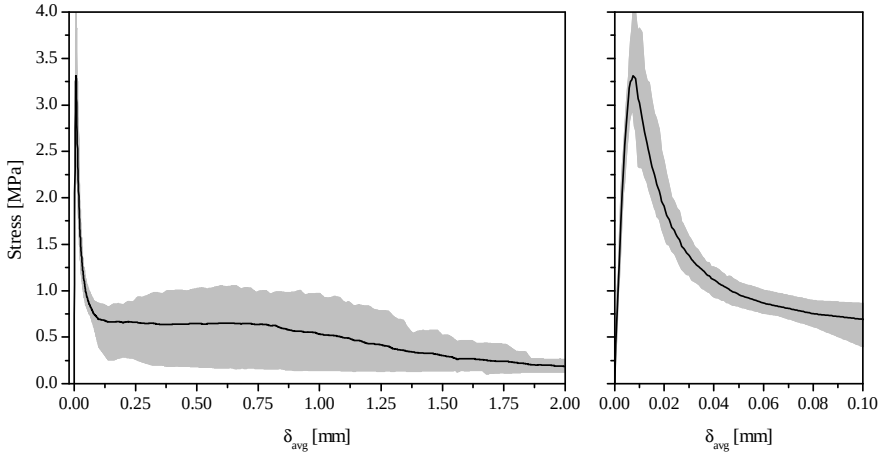

Figure 2 — Uniaxial tensile stress - displacement relationship for the Cf30 series [1 MPa = 146 psi; 1 mm = 0.0394 in]

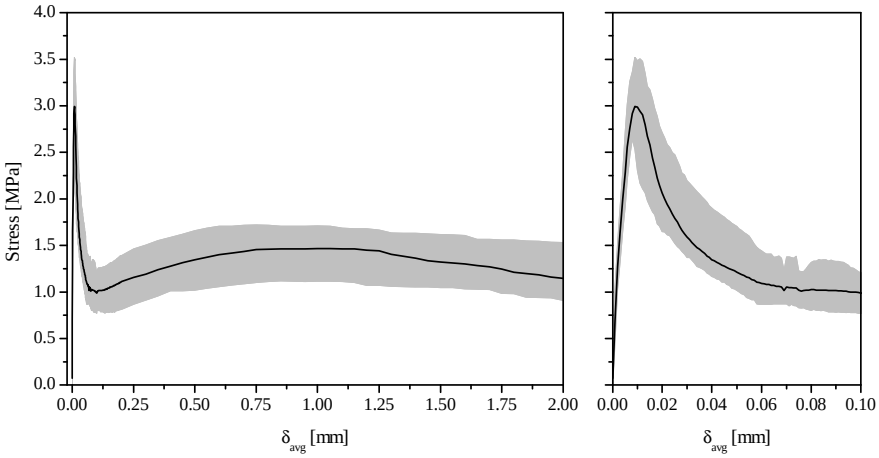

Figure 3 — Uniaxial tensile stress -displacement relationship for the Cf45 series [1 MPa = 146 psi; 1 mm = 0.0394 in]

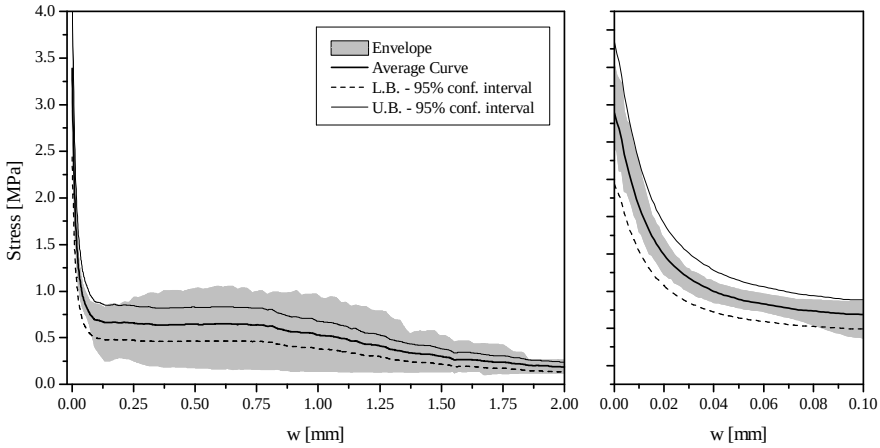

Figure 4 — Uniaxial stress - crack width relationship for the Cf30 series [1 MPa = 146 psi; 1 mm = 0.0394 in]

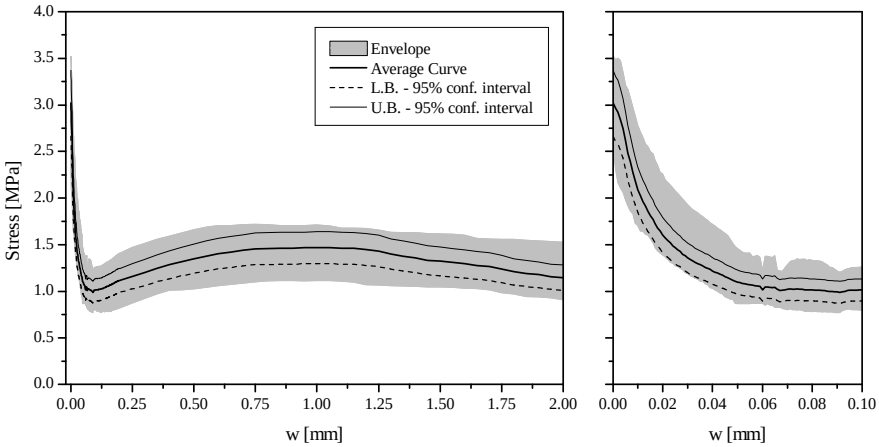

Figure 5 — Uniaxial stress - crack width relationship for the Cf45 series [1 MPa = 146 psi; 1 mm = 0.0394 in]

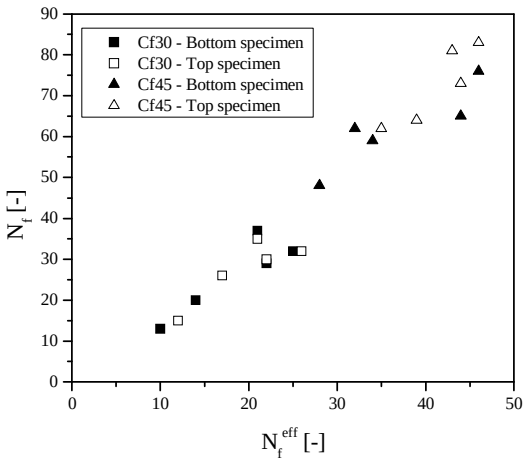

Figure 6 — Relationship between the total number of fibers and the number of effective fibers ant the crack surface

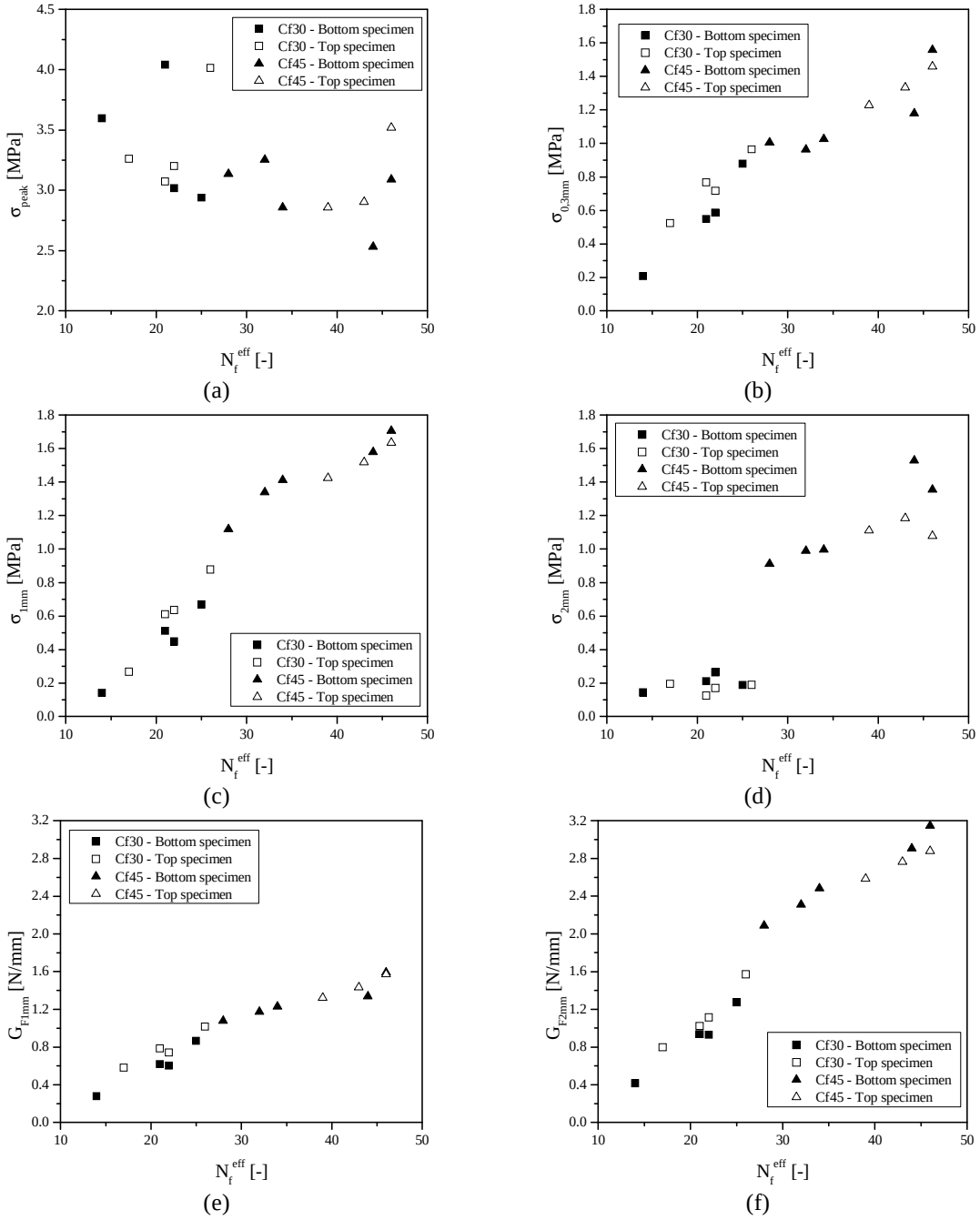

Figure 7 — Relationships between the number of effective fibers and the post-cracking parameters: (a) peak stress, (b), (c) and (d) stress at 0.3, 1 and 2 mm crack width, respectively; (e) and (f) dissipated energy up to 1 and 2 mm crack width, respectively [1 MPa = 146 psi; 1 N = 0.2248 lb; 1 mm = 0.0394 in]

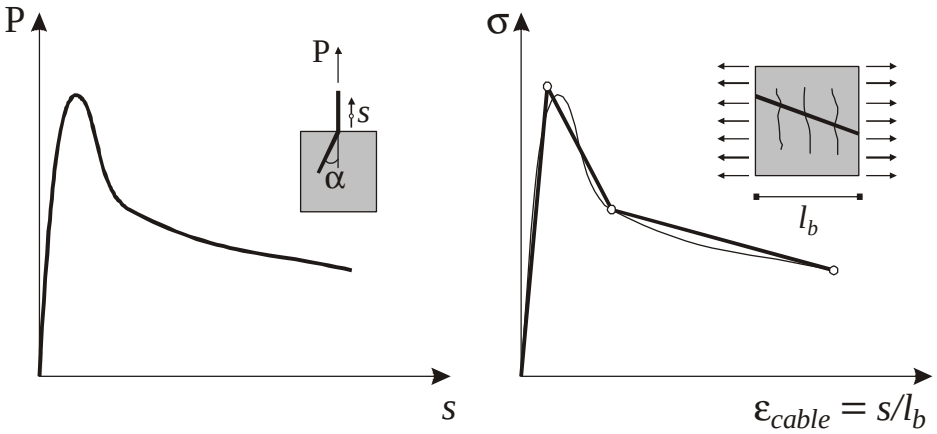

Figure 8 — Determination of the embedded cable's stress-strain diagram based on the experimental pullout force-slip relationship

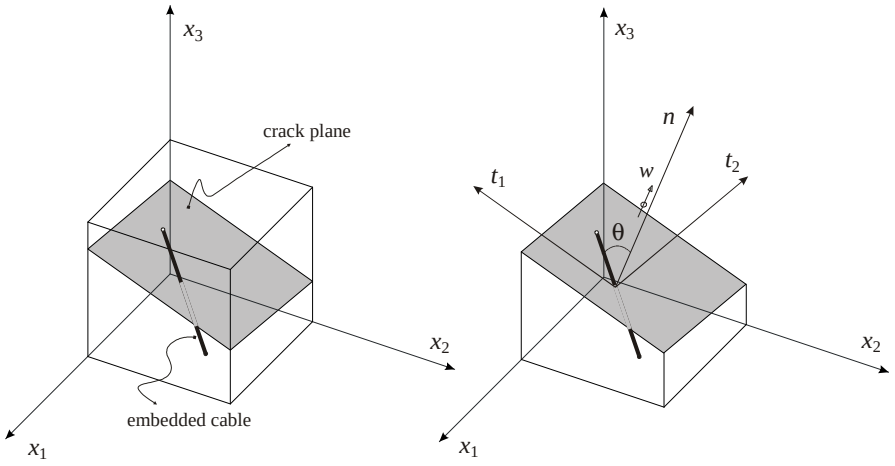

Figure 9 — Three-dimensional scheme of the embedded cable intersecting an active crack (*n* is the vector normal to the crack plane)

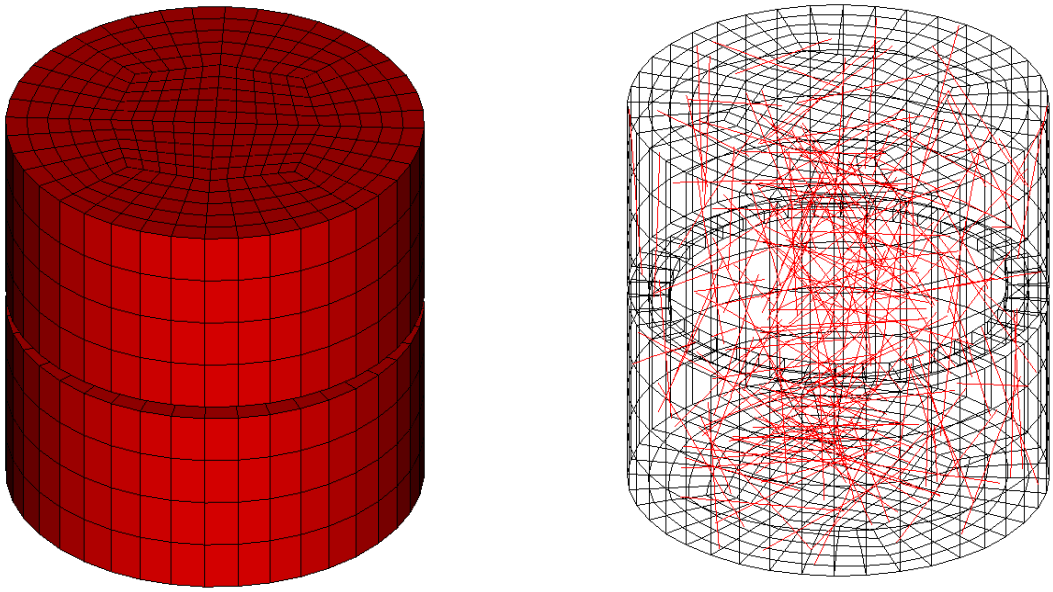

(a) ()b

Figure 10 — Three-dimensional finite element mesh: (a) concrete phase and (b) concrete + fibers phases (Cf30 series; red lines represent the fibers)

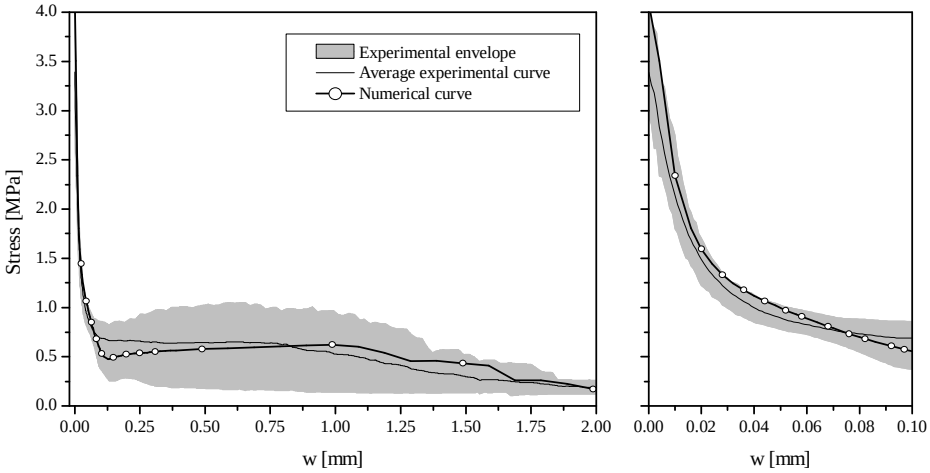

Figure 11 — Numerical simulation of the Cf30 series’ uniaxial tension tests [1 MPa = 146 psi; 1 mm = 0.0394 in]

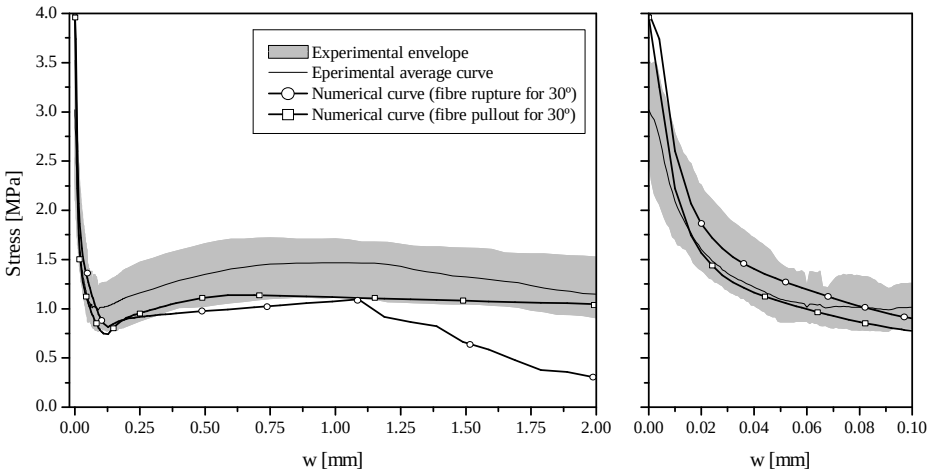

Figure 12 — Numerical simulation of the Cf45 series’ uniaxial tension tests [1 MPa = 146 psi; 1 mm = 0.0394 in]